Low-energy electron scattering from the water molecule: Angular distributions and rotational excitation

F. A. Gianturco,[a] S. Meloni, and P. Paioletti
Department of Chemistry, The University of Rome, Cittá Universitaria, 00185 Rome, Italy

R. R. Lucchese
Department of Chemistry, Texas A & M University, College Station, Texas 77843-3255

N. Sanna
Center for Supercomputing Applications to Research (CASPUR), Cittá Universitaria, 00185 Rome, Italy

(Received 25 April 1997; accepted 2 December 1997)

The scattering of electrons from the H_2O molecule in its ground electronic state is analyzed by carrying out quantum calculations of the coupled equations in the body-fixed (BF) frame and using exact static-exchange interaction forces (ESE) within a single-center expansion (SCE) formulation. The effect of correlation-polarization forces is included via a density functional approach and the necessary corrections to the nonconvergent behavior of the angular distributions from fixed nuclei calculations involving polar molecules are carried out. Elastic and rotationally inelastic differential and momentum transfer cross sections are compared with experiments and the effects on the inelastic processes of the long-range dipolar potential are examined in some detail. The electron efficiency in exciting molecular rotations over a broad range of energies is also obtained and discussed. © *1998 American Institute of Physics.* [S0021-9606(98)00610-2]

I. INTRODUCTION

The study of electron collisions with the water molecule is of fundamental importance in a great variety of research fields, such as radiation physics and radiation chemistry, atmospheric physics and astrophysics, and has been considered a topic worthy of investigation, both experimentally and theoretically, for many years. On the other hand, the theoretical development of a rigorous treatment of all the relevant scattering observables, and its numerical implementation, has been slowed down because of the special physical properties of such a molecular target, e.g., its nonlinear shape, the existence of its permanent dipole moment and the various excited electronic states which are close in energy and strongly interact with each other and with their vibrational levels. In the present paper we therefore intend to revisit the above system and to study, within our computational approach, both the influence of the long-range dipolar interaction on the behavior of the angular distributions for elastic and inelastic processes and the efficiency of the inelastic collisions with electrons that can excite the target rotor states. We will also compare the existing measured angular distributions of the scattered electrons, and some of the earlier theoretical results, with our present calculations in order to test the quality of the computational model which we are employing in the present study. The paper is organized as follows: in the next section we outline our theoretical approach while in Sec. III we analyze the behavior of the partial integral elastic cross sections and the quality of the short-range interaction as given by the present calculations. Section IV analyzes in some detail the dominant role of the long-range charge-dipole interaction and its inclusion in the scattering calculations to yield correct angular distributions which agree very well with existing experiments. Section V presents rotationally inelastic cross sections and shows their behavior over a broad range of collision energies. It also compares our present calculations with existing experiments of rotationally resolved differential cross sections. Our final conclusions are reported in Sec. VI.

The experimental angular distributions for the elastic scattering have been measured several times[1–5] and the most recent paper[5] also provides a detailed comparison between their new data and other existing measurements. While the general agreement among these data are qualitatively good, there are still some quantitative disagreements among them. The most striking one, as we shall see below, involves the determination of the corresponding integral cross sections for the elastic scattering.[6] In fact, owing to the experimental difficulties, the differential cross sections (DCS) can only be measured for angles larger than 5° and smaller than 150°. One therefore needs to resort to some extrapolation procedure to obtain the corresponding elastic integral cross sections (ICS), a procedure which invariably leads to very large uncertainties and discrepancies between the extrapolated ICS, as we shall further discuss below. Hence, we will show to be more significant for our understanding of the process to start with correctly computed and fully converged theoretical DCS values that can be more reliably compared with the measured data of the angular distributions over the same angular range.

Several theoretical studies have also been reported in recent years on the elastic scattering of electrons from the water molecule,[7–16] where the various authors have either

[a]Author to whom correspondence should be addressed. Electronic mail: FAGIANT@CASPUR.IT

employed *ab initio* methods with and without the inclusion of correlation-polarization effects[7,13,15,16] or have resorted to an entirely model treatment of exchange and correlation forces.[8–12,14] Some of the above calculations were also carried out using the single-center expansion (SCE) approach employed in the present work but with different models for the exchange and correlation forces (e.g., see Refs. 14 and 15). In general, however, one can say that the previous calculations show fairly good agreement with each other and with some of the experimental data, but not with all of them. Furthermore, they limit their comparison to the (rotationally summed) elastic differential cross sections (DCS), and the momentum transfer cross sections (MTCS), without considering specifically any state-to-state rotationally inelastic process. As we shall show below, the present set of calculations exhibits one of the best agreements with the existing DCS measurements, it employs an exact approach for the static-exchange forces, it includes an essentially converged treatment of the long-range interaction in the BF and SF frames and additionally provides information on rotationally inelastic processes which was not given by the previous theoretical treatments.

II. THE LOW-ENERGY INTEGRAL CROSS SECTIONS

We are considering here the scattering of an electron from a nonlinear molecule in the fixed-nuclei (FN) approximation. The general theory of the scattering has been presented many times before (e.g., see the review by Gianturco and Jain[17]) and therefore, in the following, only a brief outline of it will be reported. In the case of a polar molecule the partial-wave expansion of the differential cross section does not converge when evaluated in the fixed-nuclei approximation[18] and therefore one of the current procedures used to circumvent this problem is employed in the present work.

The DCS is given by the familiar expression[17]

$$q=\sum_{L} A_L(\kappa^2)P_L(\cos\,\theta), \tag{1}$$

where P_L is the Legendre function. The A_L coefficients have already been given many times before (e.g., see Ref. 17), and therefore will not be repeated here.

The T matrix is in turn defined as

$$T^{lv}_{l'v'}=\delta_{ll'}\delta_{vv'}-S^{lv}_{l'v'}, \tag{2}$$

and the corresponding integral cross section is given by

$$Q=(\pi/k^2)\sum_{lv}\sum_{l'v'}|T^{lv}_{l'v'}|^2. \tag{3}$$

It should be noted that the present cross sections, q and Q, correspond to the vibrationally elastic ones (i.e., summed over the final rotational states). In the fixed-nuclei approximation, those cross sections are independent of the initial rotational state.[18–21]

The effect of short-range correlation between the bound and continuum electrons was introduced using a global density functional theory (DFT) model already discussed before.[22–24] In that instance, the long-range part of the dipole polarizability (spherical and nonspherical) was employed to treat that region of the interaction, thereby smoothly connecting it to the short-range correlation from the DFT treatment. The full correlation-polarization (V_{cp}) interaction was therefore introduced via this parameter-free model which has already been tested successfully by us for polyatomic targets.[20–24]

III. THE ELASTIC INTEGRAL CROSS SECTIONS

We have carried out the fixed-nuclei (FN) calculations in the frame of reference of the molecule, the BF frame with the $\hat{z}$ axis along the main rotational axis of H_2O. The chosen geometry was the one given experimentally, with a bond length of 1.809 a.u. and a $\hat{HOH}$ angle of 104.50°. The computed dipole moment was 0.780 a.u. (expt., 0.728) and the quadrupole moment (Θ_{zz}) was -0.121 a.u. (expt., -0.097), while the $\Theta_{xx}-\Theta_{yy}=-3.90$ a.u. (expt., -3.82).

The single determinant (SD) wave function was of the Dunning–Huzinaga pp-cVTZ quality and yielded a total energy, at the above geometry of $-76.057\,715$ hartree. In the SCE numerical treatment we have employed a total of $220\times48\times21=221\,760$ points in the (r,ϑ,φ) polar variables. In the multipole expansion of the static potential the l_{max} value was equal to 20 and the one of the bound molecular orbitals was initially 10. In the solution of the coupled equations (3) the number of partial waves, in each of the IR for which calculations were carried out, was at first up to $l_{max}=10$, which give a maximum of 36 coupled equations in the a_1 representation where all l values were allowed. It was further extended to $l_{max}=13$, so that the convergence of the short-range interaction effects could be tested on the cross sections.

As we shall further discuss in the next section, the calculation of the K or T-matrix in any frame of reference when using the FN approximation leads to the logarithmic divergence of the integral cross section and to the divergence of the DCS in the forward direction[18] and therefore requires some modification before the integral cross sections can be reliably obtained by angular quadrature. Before that, however, it is important to also verify the convergence of the coupled equations (3) by examining, for each contributing irreducible representation (IR), the effects of improving the quality of the SCE expansion i.e. the quality of the potential coupling terms and of the bound wave functions employed during the scattering calculations.

Results on the specific behaviour of the four contributing IR's in the FN approximations are shown in Fig. 1. For each of the components the partial integral cross sections were computed at the static+exchange+polarization (SEP) treatment of the electron molecule interaction.

The dotted lines correspond to keeping $l_{max}=10$ in the coupled equations (3), while the dashed line corresponds to $l_{max}=12$. The solid lines show the results for $l_{max}=13$. One can clearly make the following comments:

(i) The results obtained with $l_{max}=13$ have essentially converged for the short-range interaction at all energies and for all the I.R.'s;
(ii) The presence of broad shape resonances is found in

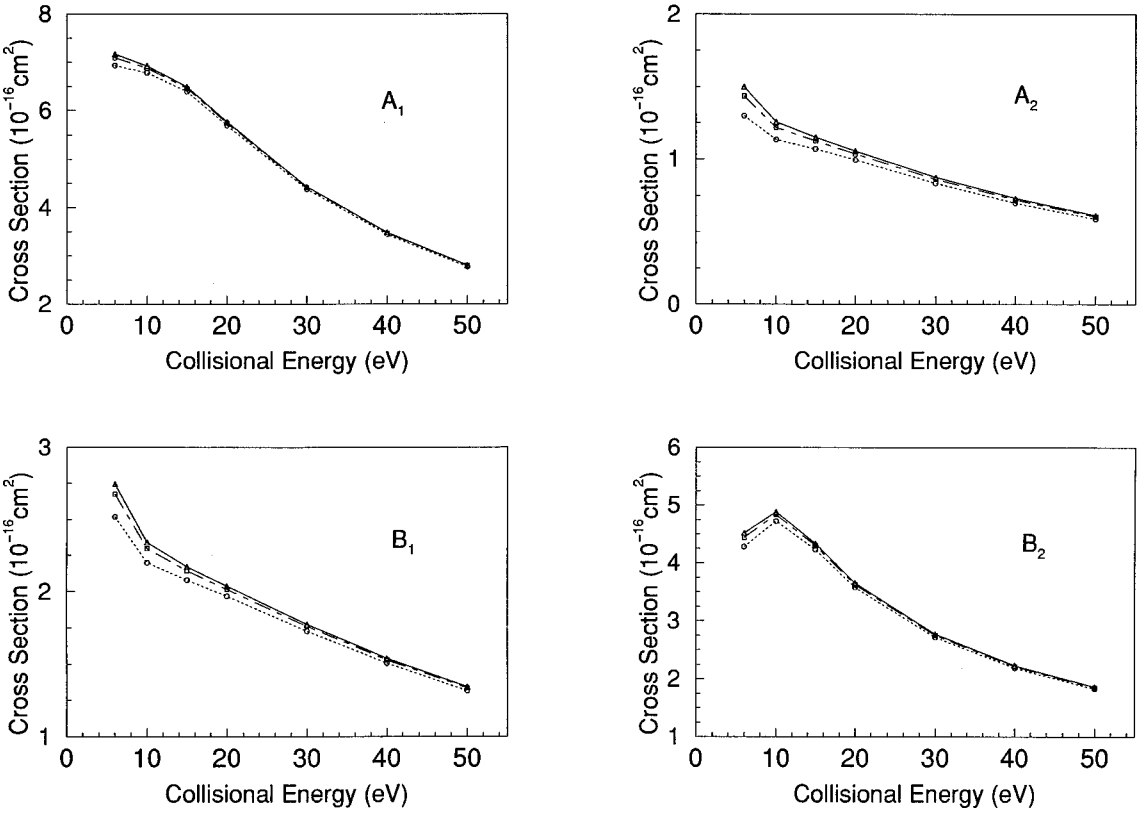

FIG. 1. Computed partial integral cross sections, at the SEP level, for the four contributing I.R.'s to the scattering from H_2O. Dotted lines, $l_{max}=10$; dashed lines, $l_{max}=12$; solid lines, $l_{max}=13$.

the A_1 and the B_2 symmetries, just below 10 eV for the former and around 15 eV for the latter. We also find that the dominant angular momentum components are $l=2$ and $l=1$ respectively, as already discussed in our earlier work;[11,25,26]

(iii) The dominant symmetry contributions to the total integral cross sections are the A_1 and B_2 components, while the B_1 and A_2 contributions are markedly smaller at all energies examined.

The SE and the SEP calculations are compared in Fig. 2 for all the I.R.'s evaluated before. One sees there that the effect of adding correlation contributions has, in general, rather little influence on the values of the final partial cross sections; the changes are mostly evident at very low energy, as expected, and mainly in the B_2 component. In the latter instance, in fact, the correlation contributions deepen the attractive potential thereby increasing the barrier which traps the metastable state. As a consequence, the resonance position moves to a lower energy and the size of the corresponding cross section increases. The global effect of correlation contributions on the integral cross sections from the CC equations is further seen in Fig. 3.

That the short-range interaction has essentially converged for the chosen SCE expansion can be gathered also from the behavior the momentum transfer cross sections presented in Fig. 4. The latter quantity is in fact given by

$$\sigma_m = 4\pi(A_0 - \tfrac{1}{3}A_1) \tag{4}$$

and therefore avoids the forward scattering divergence of the BF-FN integral cross sections.[18] The present calculations are shown in the figure by the curve marked by the stars, while the experiments[14] are given, with their error bars, by open squares. The model calculations of Ref. 14 are also reported.

The present SEP calculations describe rather well the experimental behavior and follow closely the energy dependence of the measured σ_m values. The earlier calculations of Okamoto *et al.*[14] are essentially coincident with our results at all energies, with only a minor difference at 6 eV where both calculations are smaller than the experimental data. The previous SCE calculations of Ref. 15 only evaluate MTCS up to 10 eV and are also in good accord with the present results. Similar calculations using the complex Kohn variational technique[13] yielded up to 30 eV MTCS at the ESE level which were lower than the experimental values. Their ESEP results went up to 8 eV and are very close to the present findings. Rather good accord was also obtained from the more recent calculations which employed the iterative Schwinger variational method.[16]

IV. DIPOLE INTERACTION AND ANGULAR DISTRIBUTIONS

If no approximations are made with respect to the rotovibrational molecular degrees of freedom involved in the dynamics, and all calculations are carried out in the laboratory frame, space-fixed (SF) frame of reference (for a recent review of the terminology, see Ref. 17) then the partial, state-

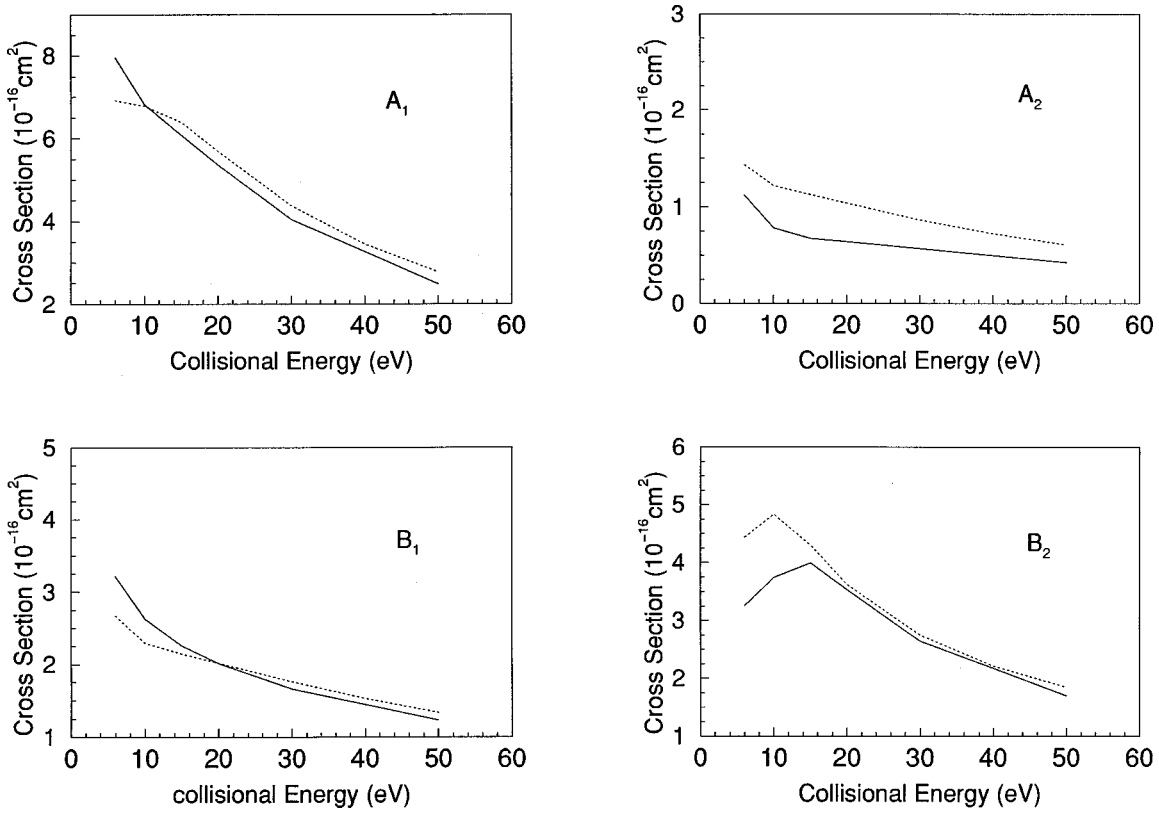

FIG. 2. Comparison between static-exchange (SE) (solid lines) and static-exchange-polarization (SEP) (dotted lines) calculations for the four I.R.'s contributing to electron scattering from H_2O molecules.

to-state differential cross section for scattering into the polar angle ϑ can be expressed as a Legendre expansion with coefficients depending on the rotational quantum numbers of the asymmetric rotor

$$\frac{d\sigma}{d\Omega}(j\tau\rightarrow j'\tau')=k'/k\sum_{\lambda}A_{\lambda}(j\tau\rightarrow j'\tau')P_{\lambda}(\cos\vartheta), \tag{5}$$

where the A_λ coefficients depend explicitly only on products of the elements of the transition matrix $\hat{T}$ and other algebraic factors.[17] Also, $k'^2=k^2+2(E_{j\tau}-E_{j'\tau'})$.

Since their precise form involves in principle infinite sums over the angular momenta (l,l') characterizing the matrix elements of $\hat{T}$, then the presence of a very long-range potential in the case of electron scattering from polar molecules implies that a very large number of A_λ coefficients need to be evaluated and therefore that a very large set of (l,l') indices of the $\hat{T}$ matrix need to be included in the exact calculations owing to the very slow convergence of the sum in Eq. (5).

In the case of polar molecules, the partial wave expansion of the cross section does not converge if the fixed-nuclei

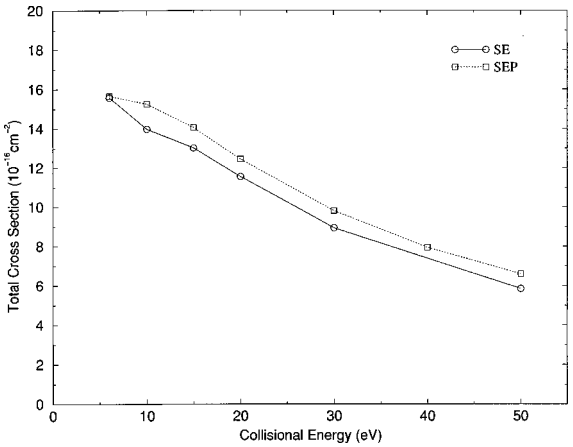

FIG. 3. Computed total integral cross sections (rotationally summed) at the SF (open circles) and at the SEP (open squares) levels of calculations by solving coupled equations in the BF frame.

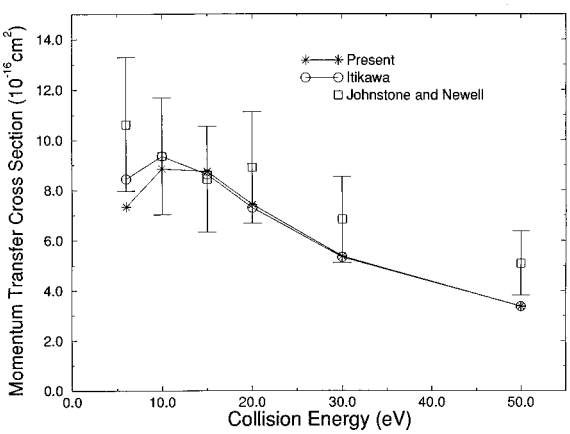

FIG. 4. Computed and measured momentum transfer cross sections as function of collision energies. Open squares, experimental points from Ref. 5. Open circles, previous calculations from Ref. 14. Stars, present calculations.

approximation is applied as it stands. To remedy this difficulty, one can use the following closure formula instead:[27–29]

$$\frac{d\sigma}{d\Omega}=q^B+\sum_L (A_L-A_L^B)P_L(\cos\,\theta). \tag{6}$$

Here the superscript B denotes that the relevant quantity is calculated in the Born approximation with an electron-point-dipole interaction. The summation over L in Eq. (6) converges rapidly, because the contribution from the higher partial waves to the DCS is dominated by the electron-dipole interaction and can be calculated in the Born approximation. The first term in Eq. (6) is then given via the formula

$$q^B=\sum_{j'\tau'} q^B_{\rm rot}(j\tau\rightarrow j'\tau'). \tag{7}$$

Here $(j\tau)$ denote the rotational state of H_2O and $q^B_{\rm rot}(j\tau\rightarrow j'\tau')$ is the Born DCS for the rotational transition $j\tau\rightarrow j'\tau'$ calculated with a point-dipole interaction from a rotor scatterer. This has in turn the following form:[30,31]

$$q^B_{\rm rot}(j\tau\rightarrow j'\tau')=\frac{4}{3}\frac{k'}{k}(2j'+1)\mu^2|\langle j'\tau'|k\tau\rangle_{100}|^2 \times(k^2+k'^2-2kk'\,\cos\,\theta)^{-1}, \tag{8}$$

where k and k' are the wave numbers of the incident and the scattered electrons and $\mu^2|\langle j'\tau'|k\tau\rangle_{100}|^2$ is the squared dipole transition moment.

The integral cross section is calculated similarly by

$$Q=Q^B+4\pi(A_0-A_O^B) \tag{9}$$

with

$$Q^B=\sum_{j'\tau'} Q^B_{\rm rot}(j\tau\rightarrow j'\tau') \tag{10}$$

and the Born cross section is given as

$$Q^B_{\rm rot}(j\tau\rightarrow j'\tau')=\frac{8\pi}{3}(2j'+1)\mu^2|\langle j'\tau'|j\tau\rangle_{100}|^2\frac{1}{k^2} \times\ln\left|\frac{k+k'}{k-k'}\right|. \tag{11}$$

It should be noted that q^B and Q^B depend on the initial rotational state $(j\tau)$ and hence q and Q do also. The above formulas can be regarded as a correction to the Born approximation treatment of dipole interaction since they include short-range effects from the CC calculations. Clark[32] already discussed this point in the case of diatomic molecules.

One can rewrite Eq. (5) in a completely equivalent form

$$\frac{d\sigma}{d\Omega}(vj\rightarrow v'j')=\frac{d\sigma^{\rm FBA}}{d\Omega}(vj\rightarrow v'j')+\Delta\,\frac{d\sigma}{d\Omega}(vj\rightarrow v'j'), \tag{12}$$

where

$$\frac{d\sigma}{d\Omega}(vj\rightarrow v'j')=\frac{1}{4k_{vj}^2}\sum_\lambda \{A_\lambda(vj\rightarrow v'j') -A_\lambda^{\rm FBA}(vj\rightarrow v'j')\}P_\lambda(\cos\,\vartheta). \tag{13}$$

Aided by cancellation, the sum over λ in Eq. (12) can now converge more rapidly and terminate for a given $\lambda_{\rm max}$ at a preselected accuracy. Thus, the first term on the right-hand side of Eq. (12) represents the result from the use of the analytic Born (AB) expression while the correction term of Eq. (12) contains first the contributions from the CC results and then subtracts from it a further term which is extracted from the unitarized Born (UB) formulation for the T-matrix, as constructed from the FBA K-matrix elements[8–11]

$$T^{\rm UB}=1-(1+iK^{\rm FBA})(1-iK^{\rm FBA})^{-1}. \tag{14}$$

One should also note that a BF formulation of the ANR was used earlier on[33–35] to provide an entirely equivalent set of correction formulas which go under the name of MEAN approximation for the divergent DCS problem in polar diatomic targets.

The final rotovibrationally (or only rotationally) inelastic cross section can then be written as

$$\frac{d\sigma^{\rm MEAN}}{d\Omega}(vj\rightarrow v'j')=\frac{d\sigma^{\rm FBA}}{d\Omega}(vj\rightarrow v'j') +\Delta\,\frac{d\sigma^{\rm MEAN}}{d\Omega}(vj\rightarrow v'j'). \tag{15}$$

The specific effects coming from the pathological behavior of the charge-dipole interactions, are shown in Fig. 5 for the four contributing I.R.'s which we have already discussed in the previous section. What we show here are the increasing contributions from higher partial waves which are added to the short-range results by including only the FBA approximation. In other words, the solid line shows the CC results with $l_{\rm max}=10$ while the three additional curves, for each I.R., show the contributions from higher $l_{\rm max}$ values coming from the FBA only and treated in the FN approach, i.e., generating partial integral elastic cross sections. The three curves correspond now to $l_{\rm max}=20$ (dotted curves), $l_{\rm max}=30$ (short-dashed curves), and $l_{\rm max}=40$ (long-dashed curves) and one clearly sees that their effect is to slowly increase the values of the integral cross sections, especially in the low energy region of the scattering. One should also note here that, if the CC equations were to be solved with $l_{\rm max}=40$, then we would have had to solve 441 coupled equations for all the I.R.'s employed.

The results reported by Fig. 6 show the total (vibrationally elastic) cross sections contributing beyond the CC results as given by the first Born FNA values for the higher (l,l') elements of the K-matrix. The number in brackets refer to the corresponding value of $l_{\rm max}$. The thick line refers to our results using the closure formulas while the dotted line reports the same calculations from Itikawa and co-workers.[14] The two corrected calculations are clearly very close to each other in spite of the differences in the short-range treatments employed by us and by the previous authors,[14] thus indicating the dominant role of dipole scattering at low energies in the present system. Our calculations also confirm a warning to the use of experimentally extrapolated integral cross sections as a test of theoretical results; given the large portion of the DCS which is contained in the small-angle region as the energy decreases, in fact, it becomes rather dubious to be

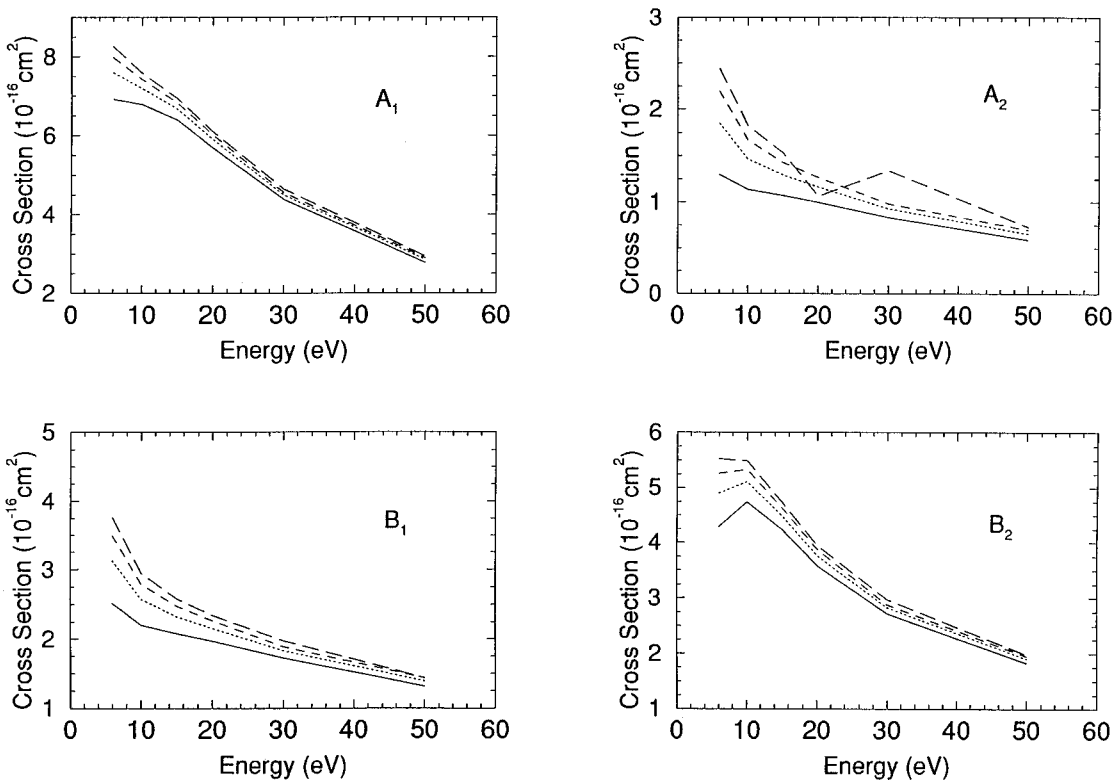

FIG. 5. Converged behavior of the computed partial integral cross sections as a function of the number of partial waves added to the CC results via the unitarized Born results of Eq. (14). Solid lines, $l_{max}=10$; dotted lines, $l_{max}=20$; short dashes, $l_{max}=30$; long dashes, $l_{max}=40$.

able to obtain such portion from empirical extrapolations only and the present comparison with the experimentally obtained cross sections (open squares and open circles),[5,36,37] makes this point clearly. The total integral cross sections from Ref. 37, given by the lozanges, show a very interesting increase at low energy which is also given by our calculations, but is not able to correctly handle the forward scattering region through simple extrapolations.

A much better test on the achieved convergence of the calculations is therefore provided by the behavior of the DCS over a range of scattering energies as broad as possible. A comparison between computed and measured values is presented in Figs. 7–9, where elastic (rotationally summed) differential cross sections are shown for collision energies of 6 eV up to 50 eV. In that comparison we show the present calculations (solid lines) one of the earlier theoretical results (dotted lines)[41] and the experimental values from Ref. 5 which are given by open squares. One can make the following comments:

(i) The agreement with the measured values is nearly perfect at all energies. Furthermore, our calculations clearly extrapolate at smaller angles and at the larger angles very reasonably without any discontinuity in our computed distributions;

(ii) Our results also follow very closely the earlier model calculations of Itikawa and co-workers.[14] Since the two sets of computed DCS are essentially coincident, it is fair to say that in the present polar molecule the role of the dipole scattering is of paramount importance, overriding at nearly all angles the effect of a better treatment of exchange and static forces at short-range provided by the present calculations. As expected, however, the better quality of our *ab initio* ESE computations comes through in the large-angle region where short-range forces are more influential and where therefore the model calculations of Ref. 14 differ most from experiments.

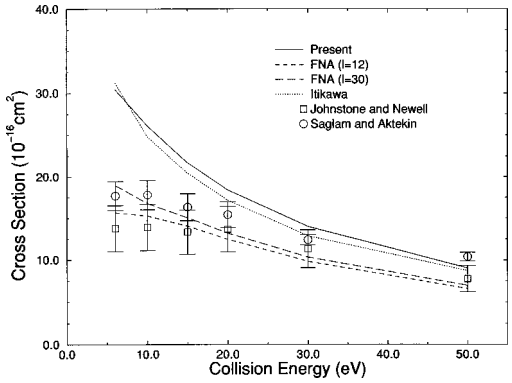

FIG. 6. Computed total integral cross sections with the contributions from Fig. 5. Short dashes, $l_{max}=12$; long dashes, $l_{max}=30$. Dots earlier calculations from Ref. 14. Thick line, present results using the MEAN approximation of Eq. (15). The experimental points are from Refs. 5 (open squares), from Ref. 36 (open circles), and from Ref. 37 (open losanges).

V. THE ROTATIONALLY INELASTIC CROSS SECTIONS

Because of the dominance of the dipole-charge interaction, the anisotropic coupling between the nuclear motion

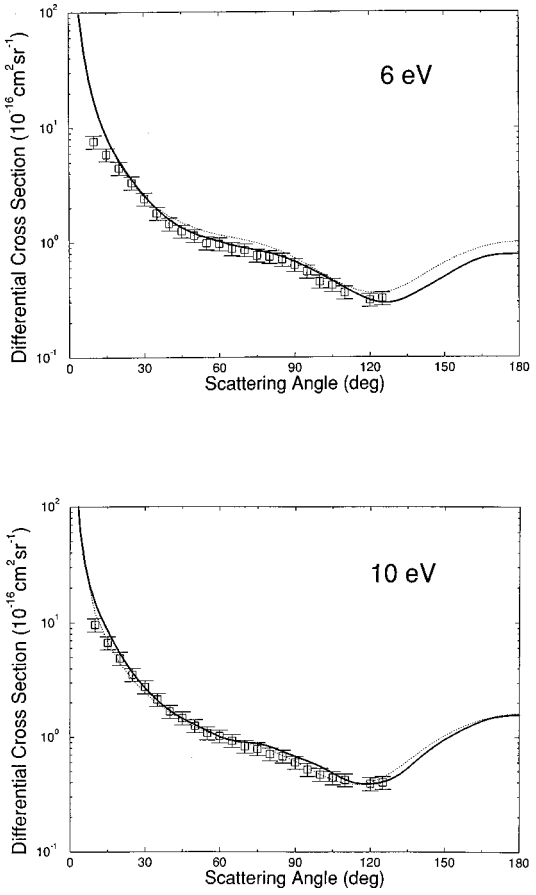

FIG. 7. Elastic (rotationally summed) differential squares sections at 6 eV (top) and 10 eV (bottom). The squares are the experimental points from Ref. 5. The present calculations are given by the solid lines while the dotted lines are the calculations from Ref. 14.

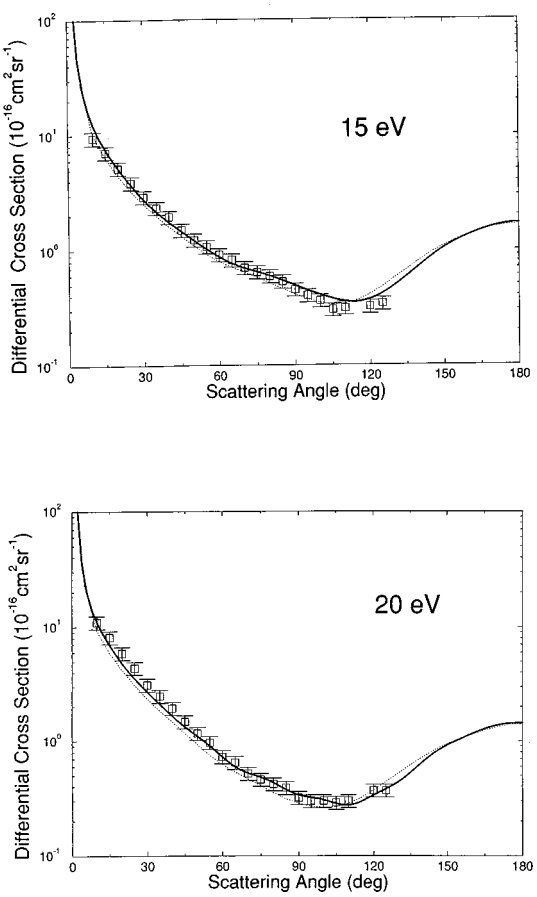

FIG. 8. Same as in Fig. 7 but for two different collision energies; 15 eV (top) and 20 eV (bottom). The notation is the same as in Fig. 7.

and the impinging electrons extends over a rather large region of space and therefore one expects efficient excitation of rotational levels by collision with electrons, in spite of the mass ratio inefficiency.[1]

The interplay of the various coupling schemes discussed briefly before could be seen by examining the angular behavior of the $(0\rightarrow 1)$ rotationally inelastic process. The rotational eigenfunctions of the H_2O asymmetric top have been already discussed before[11,35] and we will not repeat them here. Suffice it to say that by summing over the final magnetic substrates M' and averaging over initial substrates M we obtain the state-to-state differential cross sections as

$$\frac{d\sigma}{d\Omega}(J\tau\rightarrow J'\tau')=\frac{k'}{k}\sum_{M,M'}\frac{1}{(2J+1)}|f(J\tau M\rightarrow J'\tau' M')|^2, \tag{16}$$

where $|f|^2$ is the modulus of the scattering amplitude in the SF frame and the pseudo quantum number τ is introduced to distinguish the $(2J+1)$ sublevels for a given J since the projection of J along the BF axis, K, is no longer a good quantum number for an asymmetric top.[35]

By summing over the τ' quantum number and overaging over τ, in the following discussion we will label the $(00\rightarrow 10)$ as the $(0\rightarrow 1)$ transitions. Since the latter corresponds to the inelastic process dominated by charge-dipole interaction,[11] it is instructive to see how its behavior is changed by the different contributions of the previous section. As an example, Fig. 10 reports such contributions for the DCS of the $(0\rightarrow 1)$ excitation at two different collision energies; the low value of 6 eV (top) and the much larger value of 50 eV (bottom).

The following effects can be seen from the figure:

(i) The pure analytic Born cross sections (dotted lines labeled AB) show the strong peaks in the forward direction but are smoothly going to a nearly vanishing value in the backscattering region;

(ii) The close-coupling results with the $l_{\max}$ mentioned earlier (thick-dotted lines labeled CC) show instead a very marked oscillatory behavior due to the interference structures and to the lack of convergence in the partial wave sum for the long-range interaction, as shown by the strong divergence in the forward scattering region;

(iii) The unitarized Born results (the thin lines given by the UB label) are now showing the interference structures due to the same partial wave sum as in (ii) but with Born-type, A_L^B, coefficients;

(iv) As expected, the direct difference between the CC and the UB results (dashed lines labeled CC-UB) shows the disappearance of the oscillatory structure and the elimination of the forward peak; the latter feature is in

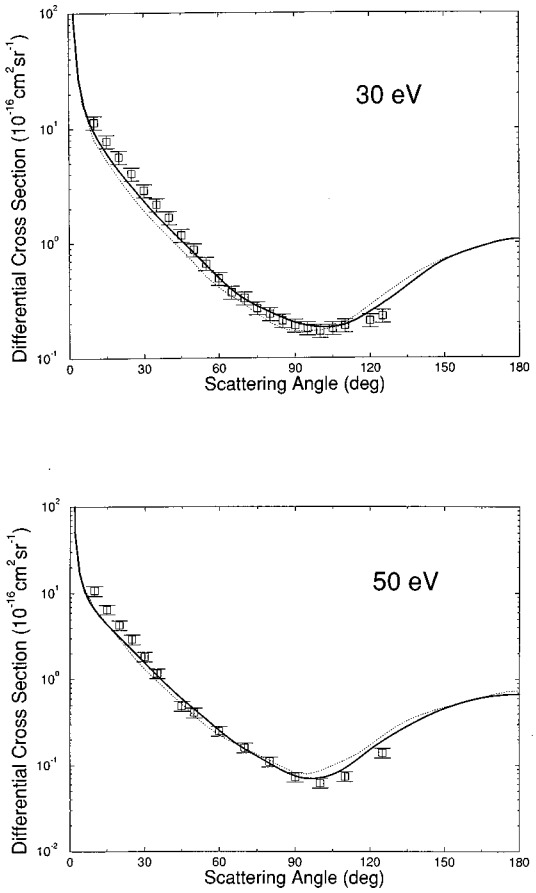

FIG. 9. Same as in Fig. 7 but for two other collision energies; 30 eV (top) and 50 eV (bottom). The notation is the same as in that figure.

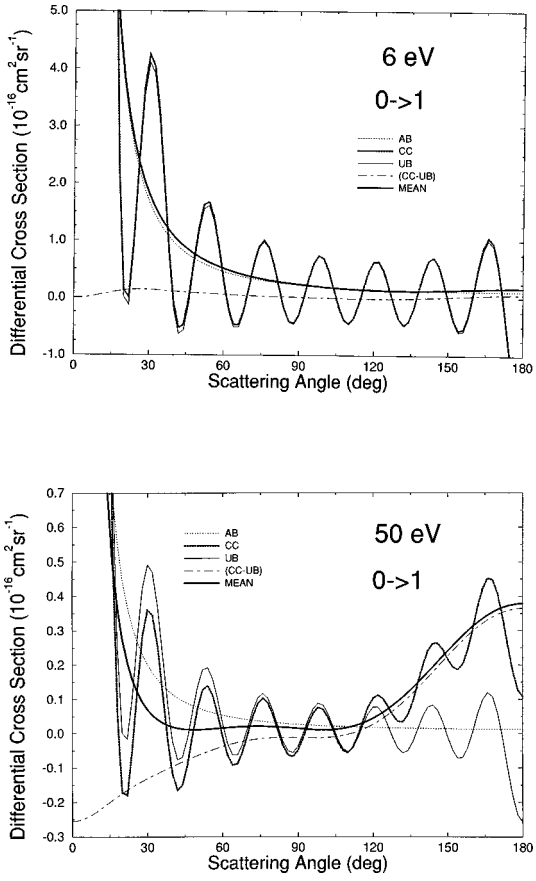

FIG. 10. Computed rotationally inelastic, partial differential cross sections for the $(0\rightarrow 1)$ excitation process. Top diagrams, at 0.6 eV. Bottom, at 50.0 eV. The notation for the various computational contributions is explained in the main text.

fact due mainly to the dipole interaction in the DCS expression from the analytic Born formula;

(v) The final sum between the contributions from (i) and (iv) yields the MEAN cross sections discussed before. Their behavior (thick solid lines) is now smooth again and shows the strong forward peak as finite. It is interesting to note that, at low energy, the AB and MEAN DC's nearly coincide at all angles while, as the energy is increased, one further sees both the presence of a back scattering contribution from the short-range interaction and the fact that MEAN and AB contributions differ from each other in the forward scattering region. Furthermore, the forward peak becomes less marked at larger E_{coll} values and starts to dominate at smaller scattering angles, as the energy increases.

The generally dominant effect of the $(0\rightarrow 1)$ transition, especially at low collision energies, is shown by the results in Fig. 11, where partial, inelastic DCS are reported at two different energies. All the calculations are now fully corrected via the MEAN formula of Eq. (15). As expected, the $(0\rightarrow 1)$ cross section is even larger than the elastic one in a small angular cone in the forward region and returns to be the largest contribution in the back scattering region.

Such a behavior is further shown by the results of Fig. 12, where we report, at different collision energies, the partial integral state-to-state cross sections over a broad range of ΔJ values. The top diagram shows the cross sections while the lower diagram reports the momentum transfer cross sections. The $\Delta J=1$ process is clearly the most likely excitation process to occur at all energies and, at the lower collision energies, it is even larger than the elastic cross section. On the other hand, as the collision energy is increased, one finds that the multiple excitations become more important since the projectile now samples further in the short-range part of the interaction.

A more direct presentation of such a behavior is shown by the results of Fig. 13, where the various partial inelastic cross sections are reported as a function of collision energy. It is interesting to note how the elastic contributions (open circles) remain smaller than the $(0\rightarrow 1)$ excitations (open squares) up to rather large energy values. Furthermore, the excitations with larger ΔJ values are only weakly dependent on the collision energy and all of them show an increase across the region of the B_2 shape resonance discussed earlier.

A comparison with existing experiments[1] is shown in Fig. 14, where we report our computed DCS for the excitation and de-excitation processes at 2.14 and 6.0 eV. The present calculations are in fair agreement with the existing experiments and appear to improve on the results from earlier model calculations,[11,15] although some doubt on the experimental accuracy exists for the larger scattering angles of the inelastic channels (crosses).[1] It is therefore interesting to

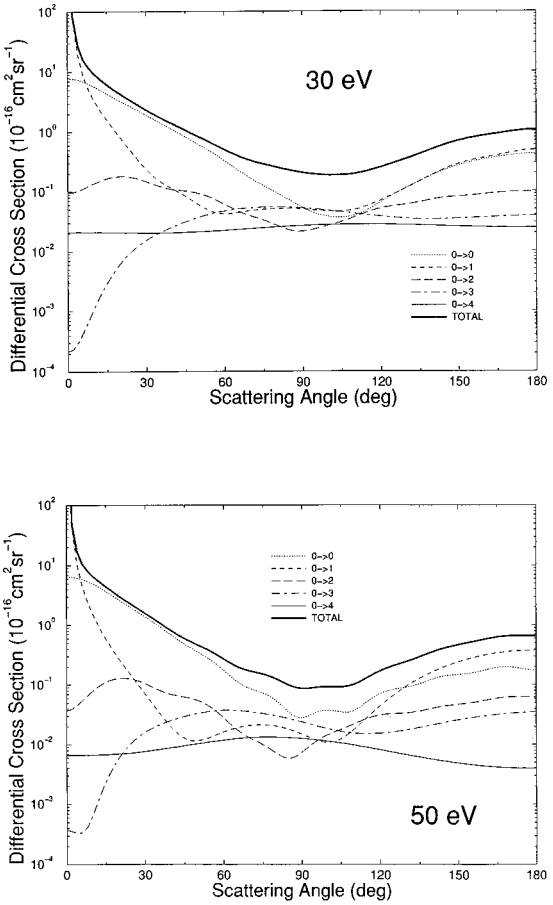

FIG. 11. Computed partial state-to-state, rotationally inelastic DCS using the MEAN approximation of Eq. (15). Top diagrams, at 30 eV of collision energy. Bottom, at 50 eV of collision energy.

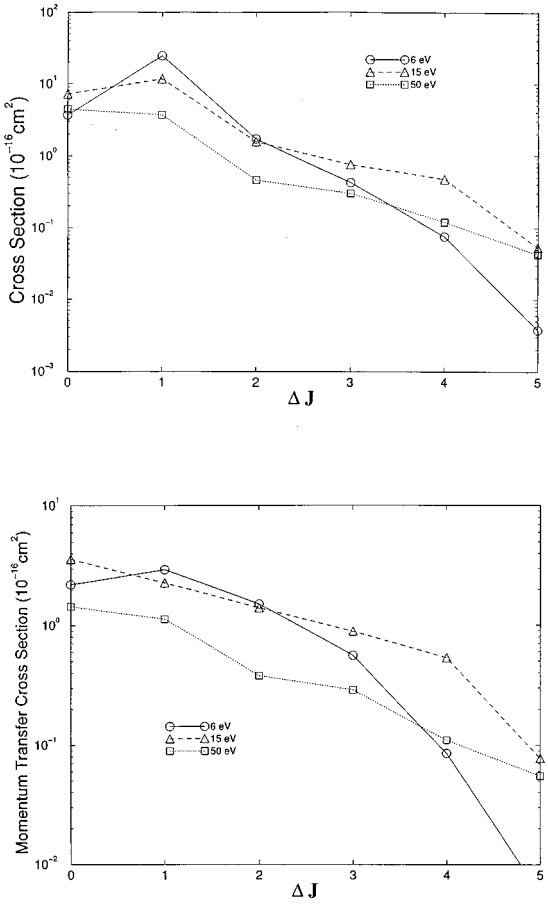

FIG. 12. Computed integral state-to-state inelastic cross sections (top) and momentum transfer cross sections (bottom) for three different collision energies and as a function of the ΔJ transition values.

compare the experimental points of the inelastic and elastic processes with different levels of computation. The upper part of Fig. 14, in fact, shows the experimental sum of the excitation and de-excitation processes $(10 \rightarrow 00)$ and $(00 \rightarrow 10)$, given by crosses. The MEAN calculations are given, for the excitation, by the solid thin line and, for the de-excitation, by the dashed thin line. Their averaged sum (as suggested by the experimental population[1]) is given by the thick solid line and follows the crosses fairly well at small angles while is below it at larger angles. The corresponding analytic Born cross sections are essentially identical to the MEAN results and suggest that, at this energy, the inelastic processes are mostly dipole-driven processes. A proof of the quality of the CC calculations in providing reliable DCS is given by the further comparison, in the same upper part of the figure, of the elastic angular distributions[1] (open circles) with the present results given by the thick dash–dotted line. The agreement is very good and confirms the quality of our CC elastic contributions. Finally, the inelastic process at lower collision energies (2.14 eV) is shown in the lower part of the figure and is compared with the analytic Born cross sections for the excitation and de-excitation processes. Their sum now follows well the experimental data and confirms the pure dipole scattering nature of the DCS at such energy, although the lowest experimental point at around 20° is surprisingly smaller than the calculations.

A quantitative presentation of our partial integral cross section is given by Table I, while the actual rotationally summed and inelastic partial DCS are available as electronic PAPS data from the American Institute of Physics.[38]

VI. GENERAL CONCLUSIONS

In the present paper we have analyzed in detail the convergence behavior of the computed cross sections, integral

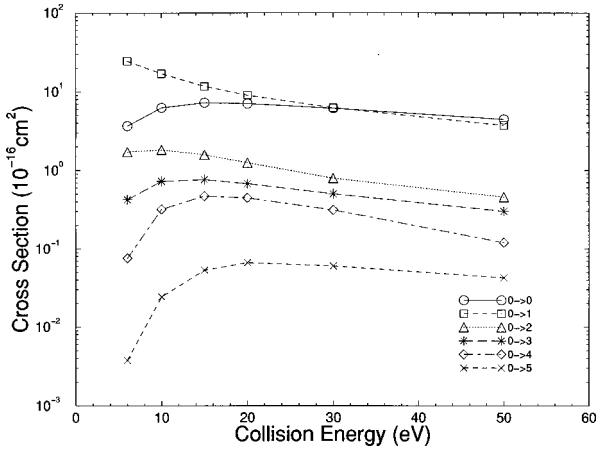

FIG. 13. Computed state-to-state inelastic integral cross sections (rotationally only) as a function of collision energies and for different ΔJ transitions.

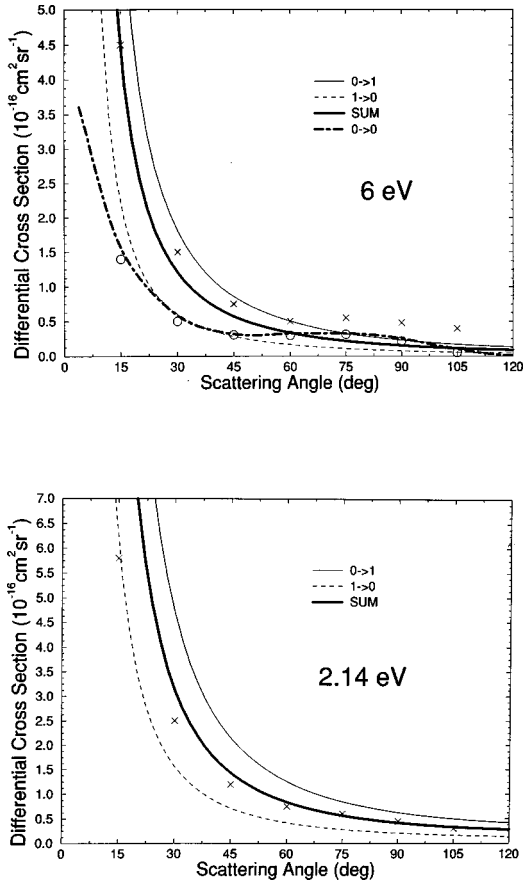

FIG. 14. Computed and measured inelastic differential cross sections at 6.0 eV (top) and 2.14 eV (bottom) of collision energies. The experimental points are from Ref. 1; the crosses correspond to the average sums of the $\{(10\rightarrow 00)+(00\rightarrow 10)\}$ processes, while the open circles correspond to the elastic processes only. See text for the meaning of the computed quantities.

and differential, for the scattering of electrons off water molecules over a broad range of energies. The calculations have been carried out using exact SE interaction and a model, parameter-free, polarization potential.

Care has been taken in checking the convergence level of the SCE expansions for the target wave function and for the multipolar interaction, together with the convergence quality of the T-matrix elements, in the BF and SF formulations, with respect to the presence of the long-range charge-dipole potential. The SF transformation has also been employed to generate for the first time the rotationally inelastic, state-to-state cross sections (integral and differential) over the same range of collision energies and to compare them with the available data at two energy values.

TABLE I. Computed state-to-state rotationally inelastic partial integral cross sections as a function of collision energy (eV). All cross sections are in units of 10^{-16} cm^2.

$0\rightarrow j$	2.14	6.0	10.0	15.0	20.0	30.0	50.0
0	25.32	3.67	6.26	7.21	7.05	6.14	4.43
1	56.83	24.50	16.96	11.68	8.97	6.23	3.71
2	5.43	1.71	1.82	1.57	1.24	0.79	0.45
3	3.03	0.42	0.72	0.76	0.67	0.50	0.30
4	0.45	0.07	0.32	0.47	0.44	0.31	0.12
5	0.03	0.004	0.02	0.05	0.06	0.06	0.04

The results of the present study, and their comparison with the available experiments, suggest the following conclusions:

(i) The light water molecule is a molecular target with only a few-electrons where the convergence of the SCE expansion of the exact static-exchange results can be achieved fairly rapidly for the short-range part of the full interaction;

(ii) The presence of the long-range charge-dipole potential dominates the elastic and rotationally inelastic scattering processes at nearly all the considered energies and the correction of its pathological divergence in the BF frame becomes an essential ingredient in the computations;

(iii) The correction via the first Born approximation appears to be fairly adequate in providing the behavior of all DCS and therefore of the ensuing integral cross sections down to very low collision energies;

(iv) Any more accurate treatment of the BF-FN short range forces turns out to be of less importance with respect to the previous correction. The present comparison with earlier calculations[14] indicates, in fact, that when the dipole interaction is correctly included it dominates the scattering process at low energies and up to fairly high collision energies;

(v) The use of integral elastic cross sections from experiments to assess quality of a given computational model is strongly dependent on the extrapolation procedure used to yield such integral cross sections. Thus, the comparison with existing measured angular distribution becomes the only reliable way for testing computational results;

(vi) Rotationally inelastic processes are dominated by the $(0\rightarrow 1)$ excitation at all energies and the latter energy-loss process is found to be larger than the corresponding elastic collisions up to fairly high scattering energies ($\leqslant 30$ eV) and to provide fairly large values of inelasticity efficiency.

ACKNOWLEDGMENTS

The financial support of the Italian National Research Council (CNR) and or the Italian Ministry for University and Research (MURST) is gratefully acknowledged. One of us (R.R.L.) also thanks a NATO Collaborative Research Grant No. C.R.G. 950552/922/94/JAR C51 for supporting his visit to Rome during the summers of 1996 and 1997.

[1] K. Jung, T. Antoni, R. Muller, K. H. Kochem, and H. Ehrhardt, J. Phys. B **15**, 3535 (1982).
[2] A. Danjo and N. Nishimura, J. Phys. Soc. Jpn. **54**, 1224 (1985).
[3] A. Katase, K. Ishibashi, Y. Matsumoto, T. Sakae, S. Maezono, E. Murakami, K. Watanabe, and H. Maki, J. Phys. B **19**, 2715 (1986).
[4] T. W. Shyn and S. Y. Cho, Phys. Rev. **36**, 5138 (1987).
[5] W. M. Johnstone and W. R. Newell, J. Phys. B **24**, 3633 (1991).
[6] O. Sueoka, S. Mori, and Y. Katayama, J. Phys. B **19**, L373 (1986).

[7] L. M. Brescansin, M. A. P. Lima, T. L. Gibson, V. McKoy, and W. M. Huo, J. Chem. Phys. **85**, 1854 (1986).
[8] F. A. Gianturco and S. Scialla, J. Chem. Phys. **87**, 6468 (1987).
[9] A. Jain, J. Phys. B **21**, 905 (1988).
[10] H. Sato, M. Kimura, and K. Fujima, Chem. Phys. Lett. **145**, 21 (1988).
[11] F. A. Gianturco, J. Phys. B **24**, 3837 (1991).
[12] J. Yuan and Z. Zhang, Phys. Rev. A , **45**, 4565 (1992).
[13] T. N. Rescigno and B. M. Lengsfield, Z. Phys. D **24**, 117 (1992).
[14] Y. Okamoto, K. Onda, and Y. Itikawa, J. Phys. B **26**, 745 (1993).
[15] R. Greer and C. Thompson, J. Phys. B **27**, 3533 (1994).
[16] L. E. Machado, L. Mu-Tao, L. M. Brescansin, M. A. P. Lima, and V. McKoy, J. Phys. B **28**, 467 (1995).
[17] F. A. Gianturco and A. Jain, Phys. Rep. **143**, 347 (1986).
[18] U. Fano and D. Dill, Phys. Rev. A **6**, 185 (1972).
[19] P. G. Burke, N. Chandra, and F. A. Gianturco, J. Phys. B **5**, 2212 (1971).
[20] F. A. Gianturco, R. R. Lucchese, N. Sanna, and A. Talamo, in *Electron Collisions with Molecules, Clusters and Surfaces*, edited by H. Ehrhardt and L. A. Morgan (Plenum, New York 1994), p. 71.
[21] F. A. Gianturco, R. R. Lucchese, and N. Sanna, J. Chem. Phys. **100**, 6464 (1994).
[22] F. A. Gianturco, R. R. Lucchese, and N. Sanna, J. Chem. Phys. **102**, 1209 (1995).
[23] F. A. Gianturco, A. K. Jain, and J. A. Rodriguez-Ruiz, Phys. Rev. A **48**, 4321 (1993).
[24] F. A. Gianturco, J. A. Rodriguez-Ruiz, and N. Sanna, J. Phys. B **28**, 1287 (1995).
[25] F. A. Gianturco, Phys. Scr. **23**, 41 (1988).
[26] F. Battaglia and F. A. Gianturco, Europhys. Lett. **10**, 117 (1989).
[27] M. A. Morrison and W. Sun, in *Computational Methods for Electron–Molecule Collisions*, edited by W. M. Huo and F. A. Gianturco (Plenum, New York, 1995), p. 152.
[28] O. H. Crawford and A. Dalgarno, J. Phys. B **4**, 494 (1971).
[29] E. S. Chang and A. Temkin, Phys. Rev. A **13**, 188 (1976).
[30] I. Itikawa, Phys. Rev. **46**, 117 (1976).
[31] L. A. Collins and D. W. Norcross, Adv. At. Mol. Phys. **18**, 341 (1983).
[32] C. W. Clark, Phys. Rev. A **16**, 1419 (1977).
[33] D. W. Norcross and N. T. Padial, Phys. Rev. A **25**, 226 (1982).
[34] D. W. Norcross, Phys. Rev. A **25**, 764 (1982).
[35] A. Jain and D. J. Thompson, J. Phys. B **16**, 3077 (1983).
[36] Z. Saglam and N. Aktekin, J. Phys. B **23**, 1529 (1990); **24**, 3491 (1990).
[37] C. Szmytkowski, Chem. Phys. Lett. **136**, 363 (1987).
[38] See AIP Document No. E-PAPS: E-JCPSA-108-006810 for the DCS values at the energies presented here in the figures. E-PAPS document files may be retrieved free of charge from our FTP server (http://www.aip.org/epaps/epaps.html) or from ftp.aip.org in the directory /epaps/. For further information: e-mail: paps@aip.org or fax: 516-576-2223.